also may be suitable for the removal of oxide impurities from other alkali chloride melts such as LiCl-KCl and KCl-NaCl.

Acknowledgment

This work was supported by the Air Force Office of Scientific Research, Grant No. 88-0307.

Manuscript submitted Nov. 30, 1992; revised manuscript received Feb. 26, 1993.

The University of Tennessee assisted in meeting the publication costs of this article.

REFERENCES

1. T. M Laher, L. E. McCurry, and G. Mamantov, *Anal. Chem.*, **57,** 500 (1985).
2. B. Gilbert and R. A. Osteryoung, *J. Am. Chem. Soc.*, **100,** 2725 (1978).
3. K. Zachariassen, R. W. Berg, and N. S. Bjerrum, *This Journal,* **134,** 1153 (1987).
4. I-W. Sun, E. H. Ward, and C. L. Hussey, *Inorg. Chem.*, **26,** 4309 (1987).
5. I-W. Sun, K. D. Sienerth, and G. Mamantov, *This Journal,* **138,** 2850 (1991).
6. I-W. Sun, K. D. Sienerth, and G. Mamantov, Unpublished results.
7. B. Gilbert, S. D. Williams, and G. Mamantov, *Inorg. Chem.*, **27,** 2359 (1988).
8. P. A. Flowers and G. Mamantov, *This Journal,* **136,** 2944 (1989).
9. P. A. Flowers and G. Mamantov, *Anal. Chem.*, **61,** 190 (1989).
10. P. A. Flowers and G. Mamantov, *ibid.*, **59,** 1062 (1987).
11. J. H. Taylor, W. S. Benedict, and J. Strong, *J. Chem. Phys.*, **20,** 1884 (1952).
12. A. H. Nielsen and R. J. Lageman, *ibid.*, **22,** 36 (1954).
13. N. B. Colthup, L. H. Daly, and S. E. Wiberley, *Introduction to Infrared and Raman Spectroscopy,* pp. 43-45, Academic Press, New York (1975).
14. J.-P. Schoebrechts, P. A. Flowers, G. W. Hance, and G. Mamantov, *This Journal,* **135,** 3057 (1988).
15. G.-S. Chen, A. G. Edwards, and G. Mamantov, *ibid.*, Submitted.
16. R. F. W. Bader and A. D. Westland, *Can. J. Chem.*, **39,** 2306 (1961).
17. B. J. Brisdon, G. W. A. Fowles, D. J. Tidmarsh, and R. A. Walton, *Spectrochim. Acta,* **25A,** 999 (1969).
18. M. Volloton and A. E. Merbach, *Helv. Chim. Acta,* **57,** 2345 (1974).
19. I-W. Sun and C. L. Hussey, *Inorg. Chem.*, **28,** 2731 (1989).
20. E. Hondrogiannis and G. Mamantov, Unpublished results.
21. C. K. Jorgesen, *Mol. Phys.*, **2,** 309 (1959).
22. E. Thorn-Csanyi and H. Timm, *J. Mol. Cat.*, **28,** 37 (1985).

Modeling of Galvanostatic Charge and Discharge of the Lithium/Polymer/Insertion Cell

Marc Doyle,* Thomas F. Fuller,* and John Newman**

Department of Chemical Engineering, University of California, and Materials Sciences Division, Lawrence Berkeley Laboratory, University of California, Berkeley, California 94720

ABSTRACT

The galvanostatic charge and discharge of a lithium anode/solid polymer separator/insertion cathode cell is modeled using concentrated solution theory. The model is general enough to include a wide range of polymeric separator materials, lithium salts, and composite insertion cathodes. Insertion of lithium into the active cathode material is simulated using superposition, thus greatly simplifying the numerical calculations. Variable physical properties are permitted in the model. The results of a simulation of the charge/discharge behavior of the Li|PEO_8-$LiCF_3SO_3$|TiS_2 system are presented. Criteria are established to assess the importance of diffusion in the solid matrix and transport in the electrolyte. Consideration is also given to various procedures for optimization of the utilization of active cathode material.

There has been interest recently in the use of thin-film rechargeable batteries for electric-vehicle applications. Several groups have developed and tested rechargeable cells incorporating a lithium anode, solid-polymer-electrolyte separator, and a composite cathode consisting of an insertion material mixed with the solid polymer electrolyte.[1-4]

Generally, large energy densities are predicted for these cells from theoretical calculations. In addition, the reversibility and large selection of materials makes insertion compounds attractive for the cathodic process.[5] Another advantage of this system is the relative safety and durability afforded by the solid separator in comparison to a liquid electrolyte.[6] The high reactivity of the lithium anode may be a significant problem; however, there is much evidence that a protective film is formed on the electrode similar to that in nonaqueous liquid electrolytes.[7] To date, experimental cells reported in the literature are small. The development of a detailed mathematical model is important to the design and optimization of lithium/polymer cells and critical to their scale-up.

There have been few previous modeling efforts of thin-film solid-state battery systems using insertion electrodes. West *et al.*[8] treated insertion into the composite cathode with porous electrode theory, modeling the electrolyte and active cathode material as superimposed continua without regard to microscopic structure (the separator was not included). Transport in the liquid electrolyte phase was described with dilute solution theory including diffusion and migration. The insertion process was assumed to be diffusion-limited, and hence charge-transfer resistance at the interface between electrolyte and active material was neglected in West's model. Data for the open-circuit potential *vs.* the amount of lithium inserted were used to relate the surface concentration of lithium in the solid matrix to the electrolyte concentration in the solution phase.

While dilute solution theory has many useful applications, an incorrect number of transport properties is defined because only interactions between the solute and the solvent are considered. Investigations of the mechanism of conduction in these electrolytes have concluded that ion pairing and ion association are important.[9] Thus, the more complete concentrated solution theory is appropriate.

Furthermore, the more rigorous theoretical framework of concentrated solution theory provides greater flexibility over dilute solution theory in accounting for volume changes and polymer flow. One also may wish to include additional species in the polymer phase, such as a low-

* Electrochemical Society Student Member.
** Electrochemical Society Active Member.

Downloaded on 2018-05-24 to IP 128.122.230.148 address. Redistribution subject to ECS terms of use (see ecsdl.org/site/terms_use) unless CC License in place (see abstract).

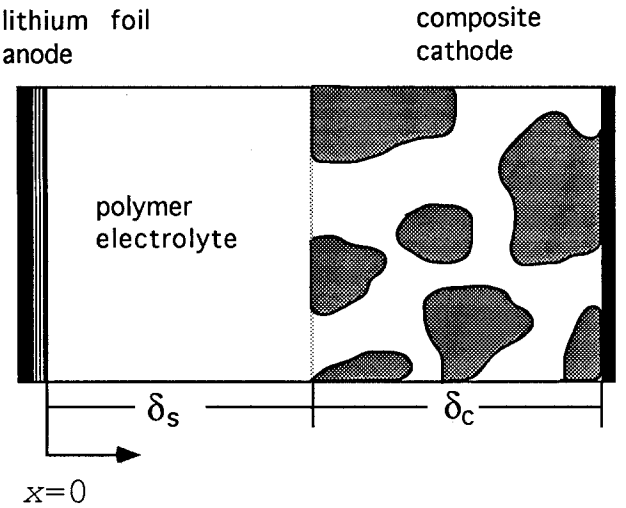

Fig. 1. Lithium/polymer cell sandwich, consisting of lithium-foil anode, solid polymer electrolyte, and composite cathode.

molecular-weight polymer phase or a second lithium salt. Treating these complexities is straightforward with concentrated solution theory.

There are limited data available on the kinetics of the charge-transfer reaction at the surface of insertion compounds. Pollard and Newman[10] have shown that the assumption of infinitely fast kinetics for a porous electrode leads to a spike in the local current density at the separator/cathode interface at short times. Assuming infinitely fast kinetics also changes the nature of the governing equations. We wish to keep the model general so that the kinetics of the cathode can be included when data are available. Consequently, a charge-transfer resistance is assumed in the present model.

An important objective of this model is to be general enough to include the full range of materials currently used in lithium/polymer/insertion systems. This generality should allow us to assess the performance of this class of battery systems in general and to establish guidelines for their optimization. Also, when data on a particular system are available, we can provide specific guidelines on cell configuration, assess the effects of kinetic and transport limitations, and evaluate the performance of the system.

Model Development

We have chosen to model the galvanostatic charge/discharge behavior of the cell sandwich shown in Fig. 1. We consider one-dimensional transport from the lithium anode through the polymer separator into the composite cathode. It is desired that the most important phenomena be treated without introducing undue complexity. Consequently, film formation at the lithium/polymer interface and volume changes during operation are ignored.

The separator consists of an inert polymer material that acts as the solvent for a lithium salt. Several polymer and salt combinations with widely varying properties have been considered in the literature.[11] Transport in the separator is modeled with concentrated solution theory, assuming a binary electrolyte and a single-phase polymer solvent. Thus the electrical conductivity, the transference number of the lithium ion, and the diffusion coefficient of the lithium salt characterize transport in the polymer. Since each of these properties is concentration dependent, variable physical properties are treated in the model. This macroscopic approach, using concentrated solution theory and variable physical properties, allows one to deal rigorously with the transport phenomena.

In concentrated solution theory (Newman, Ref. 12), the driving force for mass transfer is the gradient in electrochemical potential

$$c_i \nabla \mu_i = \sum_{j \neq i} K_{ij}(\mathbf{v}_j - \mathbf{v}_i) \qquad [1]$$

where the K_{ij} ($K_{ij} = K_{ji}$) are frictional coefficients describing interactions between species i and j. For a solution of a binary salt (*e.g.*, LiX) plus solvent (polymer), because of the Gibbs-Duhem equation, we have two independent transport equations of the form given in Eq. 1. If we use the polymer as the reference species and take its velocity to be zero, we can invert these equations to obtain

$$\mathbf{N}_+ = -\nu_+ D \nabla c + \frac{\mathbf{i} t_+^0}{z_+ F} \qquad [2]$$

and

$$\mathbf{N}_- = -\nu_- D \nabla c + \frac{\mathbf{i} t_-^0}{z_- F} \qquad [3]$$

c is the concentration of the lithium salt electrolyte ($c = c_i/\nu_i$). The K_{ij}'s can be related directly to the three measurable transport properties D, t_+^0, and κ.[13]

A material balance on the salt in the separator is then given by

$$\frac{\partial c}{\partial t} = \nabla \cdot \left(D(c) \left(1 - \frac{d(\ln c_0)}{d(\ln c)} \right) \nabla c \right) - \frac{\mathbf{i}_2 \cdot \nabla t_+^0(c)}{z_+ \nu_+ F} \qquad [4]$$

At this point we assume that the solvent concentration is not a function of the electrolyte concentration, which implies that the partial molar volume of the electrolyte is zero.[12] The variation in potential in the separator is calculated from[12]

$$\mathbf{i}_2 = -\kappa(c) \nabla \Phi_2 - \frac{\kappa(c) RT}{F} \left(1 + \frac{\partial \ln f_\pm}{\partial \ln c} \right) \left(\frac{s_+}{n \nu_+} + \frac{t_+^0(c)}{z_+ \nu_+} \right) \nabla \ln c \qquad [5]$$

where Φ_2 is measured with a lithium reference electrode. If data are available, the variation of the activity coefficient of the salt is included in this equation.

At the lithium anode ($x = 0$), a charge-transfer reaction following Butler-Volmer kinetics occurs. Following Sequeira *et al.*,[14] the reaction at the anode is assumed to take the form

$$\mathrm{Li} + \Theta_p \rightleftarrows \mathrm{Li}^+ \text{—} \Theta_p + e^-$$

where Θ_p represents a site in the polymer lattice. This corresponds to an equilibrium between occupied and unoccupied lithium sites in the solid-polymer lattice. Then we can use the exchange current density data obtained by the above authors for this reaction.

The general form of the kinetic expression is taken to be

$$I = i_{o1} \left[\exp\left(\frac{\alpha_{a1} F \eta_{s1}}{RT} \right) - \exp\left(-\frac{\alpha_{c1} F \eta_{s1}}{RT} \right) \right] \qquad [6]$$

I is the superficial current density of the cell, and η_{s1} is the local value of the surface overpotential

$$\eta_{s1} = \Phi_1 - \Phi_2 - U_1 \qquad [7]$$

U_1, the theoretical open-circuit cell potential, is zero. The exchange current density takes the form

$$i_{o1} = F(k_{a1})^{\alpha_{c1}} (k_{c1})^{\alpha_{a1}} (c_{max} - c)^{\alpha_{c1}} (c)^{\alpha_{a1}} \qquad [8]$$

The parameters k_{a1} and k_{c1} are reaction rate constants for the anodic and cathodic reactions, respectively. The total number of sites available in the polymer lattice is taken as the solubility limit of the lithium salt, denoted by c_{max}. This value is given in Appendix A for one particular lithium salt/polymer combination. The current model is easily modified to account for a simple charge-transfer process, as would be expected with a liquid electrolyte, for example. However, the experimental evidence currently available supports the above reaction stoichiometry for polymer systems.

The potential of the solid lithium phase is arbitrarily set to zero at this boundary ($x = 0$). The other boundary conditions include the flux of lithium ions equaling the net transfer of current at the interface

$$\mathbf{N}_+ = \frac{I}{F} \text{ at } x = 0 \qquad [9]$$

Downloaded on 2018-05-24 to IP 128.122.230.148 address. Redistribution subject to ECS terms of use (see ecsdl.org/site/terms_use) unless CC License in place (see abstract).

The flux and concentration of each species and the potential in the solution phase are taken to be continuous between the separator and the composite cathode material ($x = \delta_s$).

The composite cathode can consist of an inert conducting material, the polymer/salt electrolyte, and the solid active insertion particles, each of whose volume fractions should be given. These phases are treated as superimposed continua, so that a material balance on the lithium in the polymer/salt phase gives

$$\epsilon \frac{\partial(c)}{\partial t} = \nabla \cdot (\epsilon D(c) \nabla c) - \frac{\mathbf{i}_2 \cdot \nabla t_+^0(c)}{z_+ \nu_+ F} + \frac{a j_n (1 - t_+^0)}{\nu_+} \quad [10]$$

where ϵ is the volume fraction of the polymer in the cathode. The extra term here, j_n, compared to Eq. 4, is the pore wall flux of lithium ions across the interface, which is averaged over the interfacial area between the solid matrix and the electrolyte. The pore wall flux is related to the divergence of the current flow in the electrolyte phase through

$$a j_n = \frac{-s_i}{nF} \nabla \cdot \mathbf{i}_2 \quad [11]$$

The current flowing in the electrolyte phase is given by Eq. 5. Here, the diffusivity and conductivity are effective values accounting for the actual path length of the species[15]

$$\kappa_{eff} = \kappa \epsilon^{1.5}$$

and

$$D_{eff} = D \epsilon^{0.5}$$

As before, these quantities and the transference number are treated as known functions of concentration.

The boundary conditions in the solution phase are that the flux of each species is equal to zero at the cathode/current collector boundary

$$\mathbf{N}_i = 0 \text{ at } x = \delta_s + \delta_c \quad [12]$$

The active cathode material is assumed to be made up of spherical particles of radius R_s with diffusion being the mechanism of transport of the lithium. We take the direction normal to the surface of the particles to be the r-direction. Thus

$$\frac{\partial c_s}{\partial t} = D_s \left[\frac{\partial^2 c_s}{\partial r^2} + \frac{2}{r} \frac{\partial c_s}{\partial r} \right] \quad [13]$$

where c_s represents the concentration of lithium in the solid particle phase. The diffusion coefficient of lithium ions in the solid phase has been assumed constant in this expression. From symmetry

$$\frac{\partial c_s}{\partial r} = 0 \text{ at } r = 0 \quad [14]$$

The second boundary condition is provided by a relationship between the pore wall flux across the interface and the rate of diffusion of lithium ions into the surface of the insertion material

$$j_n = -D_s \frac{\partial c_s}{\partial r} \text{ at } r = R_s \quad [15]$$

As the diffusion coefficient of the inserted lithium ions is taken to be constant, this is a linear problem and can be solved by the method of superposition (see Appendix B). This is in contrast to the approach of West *et al.*[8]

This model is intended to be general enough to include a wide range of insertion compounds as the active cathode material. The open-circuit potential of insertion materials varies with the amount of lithium inserted and is expressed as

$$U_2 = U_2^\theta - U_{ref}^\theta + \frac{RT}{F} \left(\ln \left(\frac{c_T - c_s}{c_s} \right) + \beta c_s + \zeta \right) \quad [16]$$

This is similar to the expression proposed by West *et al.*[8] The only difference is the deletion of the dependence on electrolyte concentration, which is not included in this expression where the potential is defined using a reference electrode in solution at the local concentration. The parameters β and ζ can be thought of as expressing activity corrections and are taken to be constants that can be fit from experimental data on open-circuit potential *vs.* state of charge.

The insertion process at the cathode is represented by the reaction

$$Li^+ — \Theta_p + \Theta_s + e^- \rightleftarrows Li — \Theta_s + \Theta_p$$

This leads to a kinetic expression of the form

$$\mathbf{i} = F k_2 (c_{max} - c)^{\alpha_c} c^{\alpha_A} \left[c_s \exp\left(\frac{\alpha_a F}{RT} (\eta - U') \right) - (c_T - c_s) \exp\left(-\frac{\alpha_c F}{RT} (\eta - U') \right) \right] \quad [17]$$

where U' is given by

$$U' = U_2^\theta - U_{ref}^\theta + \frac{RT}{F} (\beta c_s + \zeta) \quad [18]$$

The overpotential appearing in this expression is defined as

$$\eta = \Phi_1 - \Phi_2 \quad [19]$$

Using the parameters given by West *et al.*[8] based on experimental data[a] for the TiS_2 system

$$U' = 2.17 + \frac{RT}{F} (-0.000558 c_s + 8.10) \quad [20]$$

The parameter k_2 in Eq. 17 is a combination of forward and backward rate constants for the charge-transfer reaction, similar to an exchange current density. Because the exchange current density of the charge-transfer process at the TiS_2 interface has not been reported, we set the parameter k_2 in Eq. 17 equal to a value corresponding to a nearly reversible situation. An additional condition on the potential in the insertion phase is

$$\nabla \Phi_1 = 0 \text{ at } x = \delta_s \quad [21]$$

The current flowing in the matrix is governed by

$$\mathbf{i}_1 = -\sigma \nabla \Phi_1 \quad [22]$$

The current in the two phases is conserved through

$$\nabla \cdot (\mathbf{i}_1 + \mathbf{i}_2) = 0 \quad [23]$$

leading to the integrated form

$$I = \mathbf{i}_1 + \mathbf{i}_2 \quad [24]$$

Thus, the current flows through either the polymer/salt phase or the insertion phase.

The problem now is specified completely, and the equations above are solved simultaneously using the subroutine BAND.[12] The final equations and boundary conditions are listed in Table I. The Crank-Nicolson implicit method was used to evaluate the time derivatives. About one minute of CPU time (VAX 6510) was needed to simulate a single-discharge cycle.

Results and Discussion

Appendix A gives transport properties for the polymer electrolyte. Additional parameters used in this model are listed in Table II. Quantities on the left are inherent properties of a specific system and are determined from experimental measurements. Quantities on the right may be varied to optimize a particular battery design. The porosity of the composite cathode is assumed to be constant during operation. The maximum concentration in the solid, c_T, was estimated assuming one lithium atom per molecule of titanium disulfide and using the density of TiS_2.

Figure 2 shows the cell potential as a function of utilization of cathode material for galvanostatic charge and dis-

[a] The temperature was not reported in Ref. 8. We assumed that the standard cell potential was independent of temperature.

Downloaded on 2018-05-24 to IP 128.122.230.148 address. Redistribution subject to ECS terms of use (see ecsdl.org/site/terms_use) unless CC License in place (see abstract).

Table I. Equations used in the simulation.

Variable	Equation	Boundary condition
	Separator	
c	$\frac{\partial c}{\partial t} = \nabla \cdot D\nabla c - \frac{\mathbf{i}_2 \cdot \nabla t_+^0}{z_+ \nu_+ F}$	$\mathbf{N}_+ = I/F$ at $x = 0$
η	$\nabla\eta = \frac{I}{\kappa} + \frac{RT}{F}\left(\frac{s_+}{n\nu_+} + \frac{t_+^0}{z_+\nu_+}\right)\nabla \ln c$	—
	Composite cathode	
c	$\epsilon\frac{\partial c}{\partial t} = \nabla \cdot (\epsilon D \nabla c) - \frac{\mathbf{i}_2 \cdot \nabla t_+^0}{z_+\nu_+F} + \frac{aj_n(1 - t_+^0)}{\nu_+}$	$\nabla c = 0$ at $x = \delta_s + \delta_c$
η	$\nabla\eta = \frac{-(I - \mathbf{i}_2)}{\sigma} + \frac{\mathbf{i}_2}{\kappa} + \frac{RT}{F}\left(\frac{s_+}{n\nu_+} + \frac{t_+^0}{z_+\nu_+}\right)\nabla \ln c$	$\nabla\eta = -I/\sigma$ at $x = \delta_s + \delta_c$
$\mathbf{i}_2$	$aj_n = \frac{-s_1}{nF}\nabla \cdot \mathbf{i}_2$	$\mathbf{i}_2 = I$ at $x = \delta_s$
c_s	$j_n = -D_s\int_0^t \frac{\partial c_s}{\delta t}(R_s, \zeta)\frac{\partial \bar{c}_s}{\partial r}(R_s, t - \zeta)d\zeta$	—
j_n	Eq. 17	—

charge. The utilization is

$$u = \frac{c_{s,avg}}{c_T} \quad [25]$$

The dashed line is the open-circuit potential calculated from Eq. 16, and the current density is a parameter. It is apparent that the material utilization is limited at higher discharge rates. For instance, at a rate of 20 A/m^2 the cell potential drops sharply when about 30% of the cathode material is utilized. Similar results have been observed in experimental discharge curves.[3,17] A typical cutoff voltage is about 1.7 V; beyond this value the cell is severely polarized.

The concentration of the electrolyte over the time scale of a full discharge cycle is depicted in Fig. 3. For a positive current density, the concentration at the anode increases with time as lithium is discharged into the electrolyte. The concentration changes rapidly at first, and then the concentration profiles are nearly constant over most of the discharge cycle. At long times, the concentration at the back of the cathode is low. At the front of the cathode, $x = 0.33$, the concentration dips for short times. This effect is easier to see in Fig. 4, where concentration profiles at short times are displayed.

One improvement that should suggest itself immediately when examining Fig. 3 is a change in the initial concentration of electrolyte in the cell. The use of a one molar solution is presumably due to the conductivity maximum that occurs at approximately this concentration. However, Fig. 3 shows that the bulk of the composite cathode is at a significantly lower concentration, where the conductivity is also much lower as a result. This leads to severe transport limitations in the depth of the electrode. A higher initial concentration leads to a somewhat lower conductivity in the separator but a much larger conductivity in the composite cathode, where this is of prime importance.

An important factor in optimizing the performance of the cell is good utilization of the active cathode material. For a specified battery performance, the cell potential should fall below its cutoff value only after nearly all the active material is consumed. This requires an understanding of the transport limitations in each phase of the composite cathode, as these lead to nonuniform reaction distributions.

The importance of diffusion in the solid can be assessed from the dimensionless parameter S_c

$$S_c = \frac{R_s^2 I}{D_s F(1 - \epsilon)c_T\delta_c} \quad [26]$$

and is the ratio of diffusion time to discharge time. For $S_c << 1$, diffusion can be neglected. Substitution of the parameters from Table I into Eq. 26 with $I = 10$ A/m^2 gives $S_c \approx$

Table II. Parameters used in the TiS_2 simulation.

	System specific		Adjustable	
Parameter	Value	Ref.	Parameter	Value
D_s	5.0×10^{-13} m^2/s	16	T	100°C
σ	1.0×10^4 S/m	—	δ_s	50 μm
$i_{o,1}$	12.6 A/m^2	14[b]	δ_c	100 μm
α_a, α_c	0.5	[a]	R_s	1.0 μm
ν_+, ν_-	1	—	c^0	1000 mol/m^3
c_T	29,000 mol/m^3	—	ϵ	0.3
k_2	10^{-10} m^4/mol · s	[a]	—	—
n	1	—	—	—

[a] Data are not available for these parameters.
[b] Value given is at initial conditions.

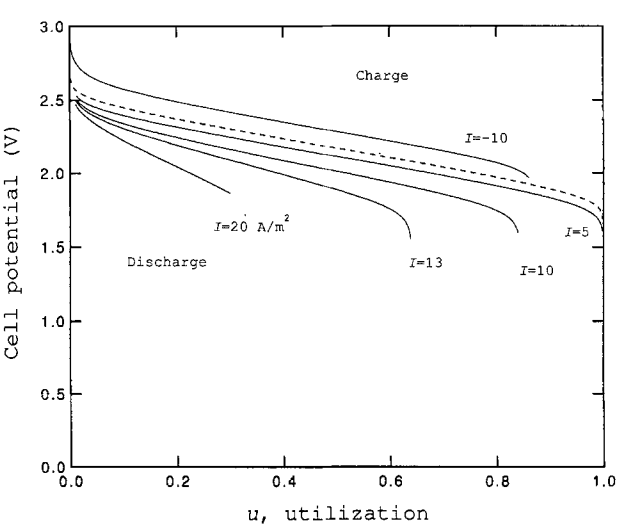

Fig. 2. Cell potential *vs.* utilization of active cathode material. *I*, the superficial current density of the cell, is a parameter. The dashed line is the open-circuit potential. For discharge curves, the initial concentration in the solid was 1% of maximum. The charging curve assumed an initially uniform utilization of cathode material.

Downloaded on 2018-05-24 to IP 128.122.230.148 address. Redistribution subject to ECS terms of use (see ecsdl.org/site/terms_use) unless CC License in place (see abstract).

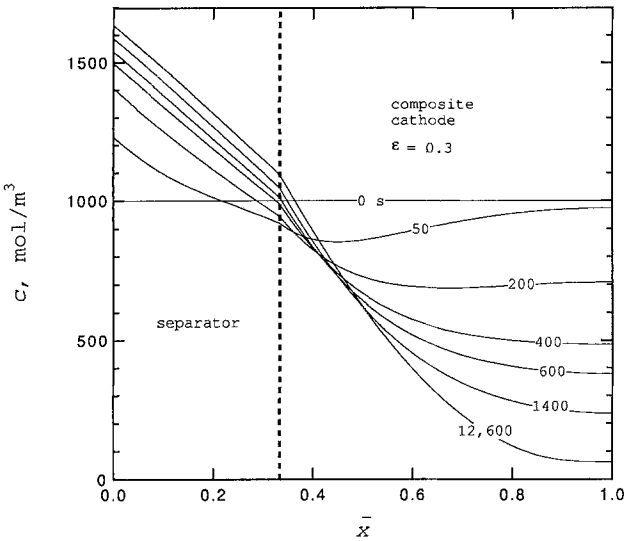

Fig. 3. Concentration profiles at long times; $I = 10$ A/m² discharge. Dashed line divides the separator and composite cathode. Initial concentration is 1000 mol/m³.

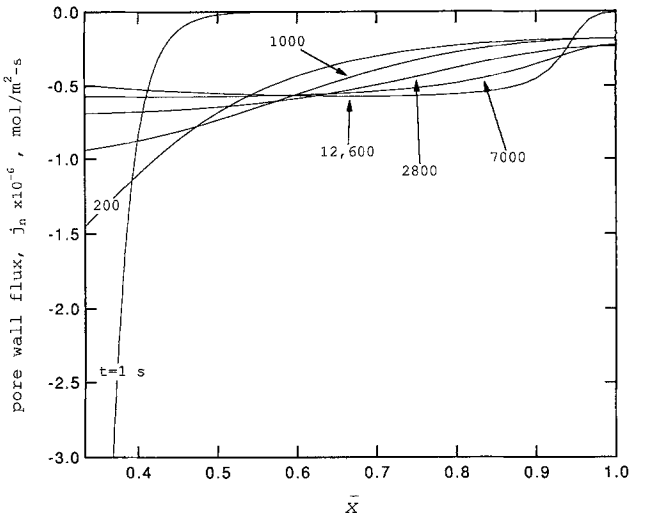

Fig. 5. Pore wall flux of lithium as a function of dimensionless distance from the anode. $I = 10$ A/m². Negative values of j_n are for insertion.

0.0001. Therefore, the concentration at the surface and the average concentration in the solid are nearly identical, and we do not present concentration profiles in the solid. Note that the radius of the particles would have to be on the same order as the thickness of the cathode for diffusion limitations to exist in the solid phase in this system. Alternatively, if the diffusion coefficient in the solid were decreased, diffusion limitations could become important.

An analogous parameter can be calculated relating the time constant for transport of the electrolyte to the time of the discharge

$$S_s = (\delta_s + \delta_c)^2 \frac{I}{DF(1-\epsilon)c_T\delta_c} \quad [27]$$

For $I = 10$ A/m², we find that $S_s = 0.15$. At high current densities, the low rate of transport in the electrolyte phase is the main factor causing the sharp drop in cell voltage at less than complete utilization of the cathode. The solution is depleted of electrolyte which cannot be replenished because of transport limitations. Therefore, for $I = 20$ A/m², the cell potential drops off at a low value of utilization of active material. This parameter also affects the concentration dip in Fig. 4 mentioned above. If transport in the electrolyte phase were the dominant limiting factor, that is $S_s >> 1$, the dip in concentration would be more pronounced and would propagate through the cathode.

Figure 5 shows the local pore wall flux of lithium ions across the composite cathode at various times during discharge. This figure is analogous to a graph of the current distribution for the system. Newman[12] gives four dimensionless parameters that characterize the current distribution in a porous electrode. These parameters describe the balance between ohmic and kinetic limitations, but not concentration effects. At short times, the concentration of electrolyte is nearly constant, and these parameters can be used to describe the current distribution.

The dimensionless current density and exchange current densities are

$$\delta = \frac{\alpha_a F I \delta_c}{RT}\left(\frac{1}{\kappa} + \frac{1}{\sigma}\right) \quad [28]$$

$$\nu^2 = (\alpha_a + \alpha_c)\frac{Fai_o\delta_c^2}{RT}\left(\frac{1}{\kappa} + \frac{1}{\sigma}\right) \quad [29]$$

If either of these parameters is significantly larger than unity, then we expect that the ohmic drop dominates the current distribution in the porous electrode. The exchange current density in the cathode can be determined from the reaction rate parameter k_2 through

$$i_{o2} = F(k_2)(c_{max} - c)^{\alpha_{c2}}(c)^{\alpha_{a2}}(c_T - c_s)^{\alpha_{a2}}(c_s)^{\alpha_{c2}} \quad [30]$$

For these calculations, the concentrations are taken to be at their initial values. In our case, we find that $\delta = 1.95$ and $\nu = 68$, and we expect the ohmic drop to dominate at short times. This is understandable when considering the reversibility usually ascribed to the charge-transfer process for insertion materials. When ohmic effects dominate, the reaction distribution can be characterized by the ratio of the electronic conductivity in the insertion material to the ionic conductivity in the polymer electrolyte. This ratio is $O(10^5)$ for this system, causing the reaction to occur preferentially at the front of the electrode. This analysis is supported by the short-time current distributions shown in Fig. 5.

As the discharge proceeds and the active material in the front of the cathode begins to fill up, the reaction shifts towards the center of the electrode. This is an effect of concentration polarizations in both the solid and electrolyte phases. In this case the predominant cause is the solid phase concentration, as a relatively small increase in the concentration in the solid has a large effect on the potential at the start of the discharge (Eq. 16). The reaction rate initially increases at the back face of the electrode, but because of transport limitations in the electrolyte phase it

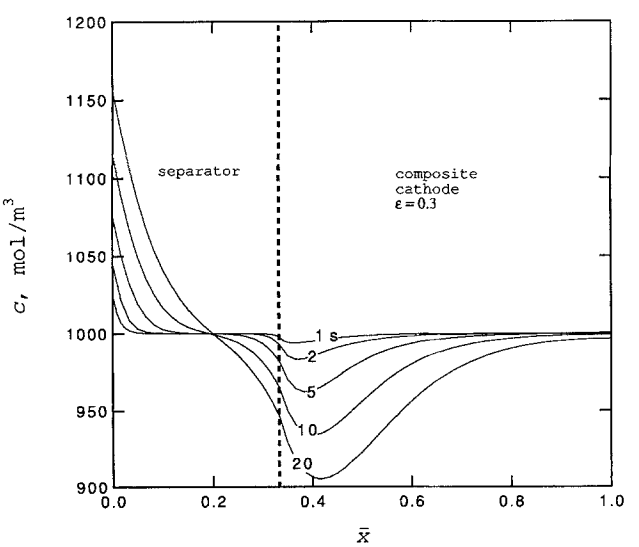

Fig. 4. Concentration profiles at short times. $I = 10$ A/m². Dashed line divides the separator and composite cathode. Initial concentration is 1000 mol/m³.

Downloaded on 2018-05-24 to IP 128.122.230.148 address. Redistribution subject to ECS terms of use (see ecsdl.org/site/terms_use) unless CC License in place (see abstract).

tapers off at long times. Figure 3 shows that the concentration in the electrolyte phase rapidly decreases at the back face. The degree to which the concentration is depleted at the back of the cathode depends on the transference number of lithium, the diffusion coefficient, and the current density.

Predicting the current distribution at long times is a more difficult problem because of the ubiquitous nature of the effect of concentration. Not only does the depletion of the electrolyte cause concentration polarizations to occur, but it also affects the kinetic expression and the transport properties. For example, in this system the transference number rapidly decreases with concentration (Appendix A), approaching zero in the depleted region near the back face of the electrode. This contributes to the poor utilization of material that is seen in this region.

For a given rate of discharge, one should be able to optimize the performance of a system by examining the reaction distribution in the electrode, Fig. 5, along with a graph of the local utilization of active material. Figure 6 shows the local utilization, which is proportional to the average concentration in the intercalation material in the r-direction. This figure allows one to examine the relationship between electrode thickness and active material utilization.

One optimization scheme is to vary the thickness and porosity of the cathode while holding its theoretical capacity constant. This could lead to a maximum in utilization when the transport limitations in the electrolyte phase are minimized. The use of this method for the current system led to the conclusion that, for a current density of 10 A/m^2 and a separator thickness of 50 μm, there is a maximum in utilization at a porosity of 0.60. This value resulted in a utilization of 97% of the active material before the cutoff potential was reached, significantly higher than the 84% that was obtained previously with a porosity of 0.30.

In general, thinner electrodes make better use of active material when transport limitations in the electrolyte exist. This does not consider the disadvantages that may be associated with processing ultrathin composite electrodes. There also would be a weight increase with many thin cells in comparison to fewer thicker cells. This is an optimization problem that requires detailed information on the battery configuration, energy and power density requirements of the system, and cost of components; these issues are not discussed here.

A general assessment of the performance of this system can be made by calculating the average and peak power for

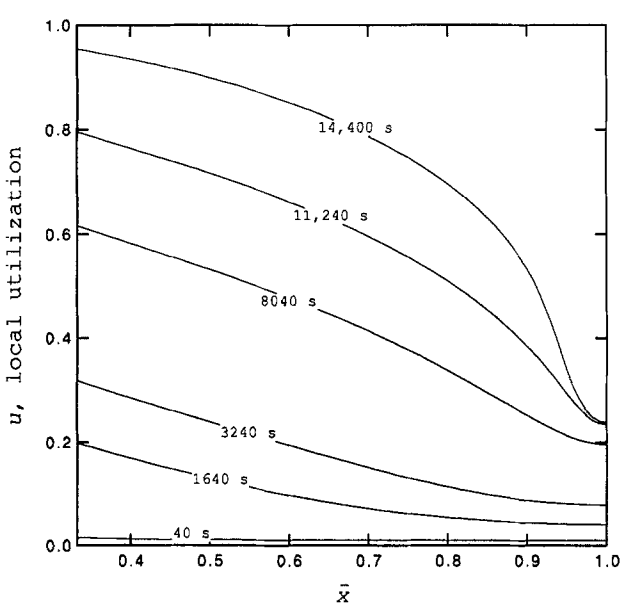

Fig. 6. Local utilization of intercalation material in the cathode as a function of dimensionless distance from the anode. Current density is 10 A/m^2.

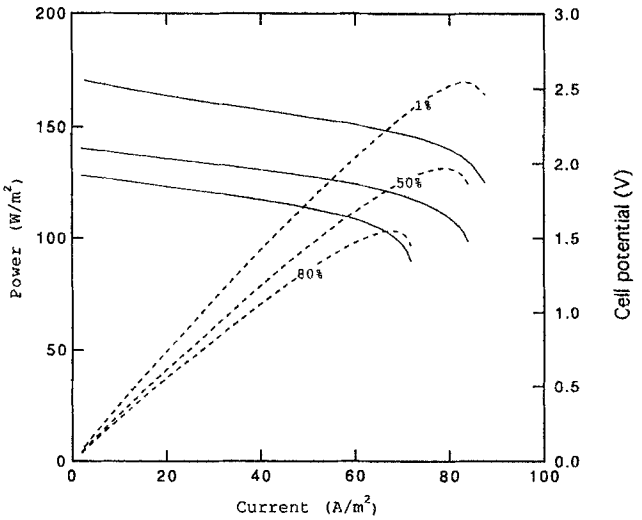

Fig. 7. Power at 1, 50, and 80% of discharge at the 3-h rate (12.1 A/m^2) as a function of current density is shown by the dashed lines. Corresponding cell potential curves are depicted by the solid lines.

a given discharge rate predicted by the model. Using a 3 h discharge rate (12.1 A/m^2), we determine the power available for a 30 s pulse of current. The power and cell potential are plotted in Fig. 7 at different depths of discharge. The values in Fig. 7 could be converted to W/kg from an estimate of the mass of material and size of the system. Basing calculations only on the mass of active cathode material used, the present simulation predicts average specific power to be 90.8 W/kg and peak power to be about 450 W/kg at 1% depth of discharge dropping to 105 W/kg at 80% depth of discharge. This represents a maximum of 1.67 h^{-1} for the ratio of peak power to average specific energy, which is lower than that desired for electric-vehicle applications. Generally, one would want this ratio to be approximately 2 to 4, depending on the desired performance and range of the vehicle. The predicted specific energy for this system is 272.4 Wh/kg.

Several improvements have been made to the model of West *et al.* of the insertion cathode, the most important being the consideration of the full cell sandwich. We also chose to model a solid-polymer-electrolyte system, while West's simulation was for a liquid electrolyte. One can first analyze the validity of their assumption that the concentration of electrolyte at the separator/cathode interface is constant. From Fig. 3, it is apparent that this concentration varies by about 15% from its initial value for the present system. Fixing the concentration at this boundary is a nonphysical condition, as it violates the principle of conservation of mass for the electrolyte. To compare discharge curves directly, we have run a simulation using the same parameters as in the West model,[8] including constant physical properties for a lithium perchlorate/propylene carbonate electrolyte. The comparison of discharge curves can be seen in Fig. 8, for a separator thickness of 100 μm.

Although the separator is an additional ohmic resistance, correcting the nonphysical boundary conditions of West's model causes a significant improvement in the performance of the system. The concentration gradients that develop in the separator provide an extra driving force for transport of the electrolyte. Whereas the earlier model predicted severe electrolyte depletion in the interior region of the porous electrode, this does not occur in the current simulation. The final material utilization predicted for the system has been increased from 80 to nearly 100% by using the correct boundary condition at the separator/cathode interface.

The current model gives a theoretical simulation of the charge or discharge behavior of a given lithium/polymer/insertion system for a single cycle. The program could be

Downloaded on 2018-05-24 to IP 128.122.230.148 address. Redistribution subject to ECS terms of use (see ecsdl.org/site/terms_use) unless CC License in place (see abstract).

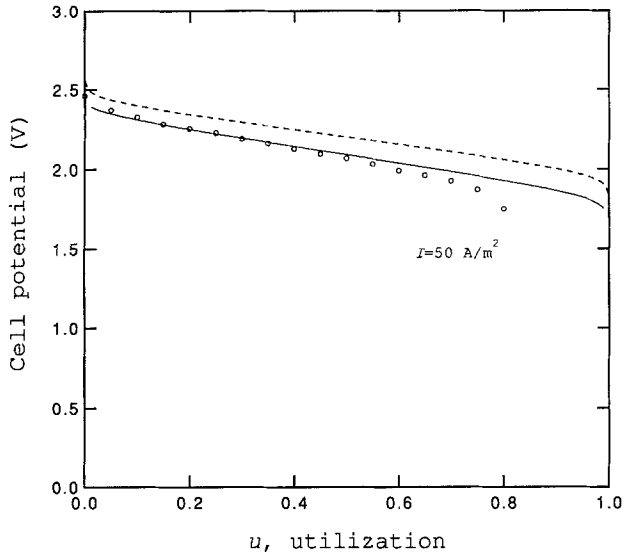

Fig. 8. Comparison of our model results with those of West *et al.* Dashed line represents the open-circuit potential. The circles are the simulation results of West *et al.*, and the solid line depicts our results.

used to predict multiple discharge and charge cycles; however, the only differences between successive cycles would be the result of concentration gradients in the cell and the differing local states of charge in the solid particles. This could be used to predict the effect of relaxation time between charge and discharge, for example.[18]

Long-term degradation of the cell due to irreversible reactions or loss of interfacial contact is not predictable under the current model. Losses of contact between the various phases of the composite cathode would be expected to occur during extended cycling. This represents a major problem in the fabrication and operation of these systems, but is beyond the scope of the present model.

Summary

A full cell model is presented for a lithium anode, solid polymer electrolyte, and insertion composite cathode. The model treats the electrolyte as a binary salt plus polymer solvent using concentrated solution theory. The velocity of the polymer is assumed to be zero and volume changes in the system are neglected. Film formation at the lithium/polymer interface also is neglected. The composite cathode is modeled using porous electrode theory with both kinetic and diffusional resistances to solid phase transport. This model is intended to give a general comprehensive treatment to the major phenomena involved in this class of systems, while providing the flexibility for secondary phenomena to be considered in the future.

Simulation results are presented for one particular polymer/salt combination using data taken from the literature. Concentration profiles and discharge curves are given and analyzed to determine the behavior of the cell during discharge. Various methods of optimizing the system parameters are discussed, with several conclusions made involving the limitations of the system.

Acknowledgment

This work was supported by the Assistant Secretary for Conservation and Renewable Energy, Office of Transportation Technologies, Electric and Hybrid Propulsion Division of the U.S. Department of Energy under Contract No. DE-AC03-76SF00098.

Manuscript submitted Oct. 30, 1992; revised manuscript received Jan. 12, 1993.

The University of California assisted in meeting the publication costs of this article.

APPENDIX A

Transport Properties

We chose to model the polymer-electrolyte system consisting of polyethylene oxide-lithium trifluoromethane sulfonate (PEO-$LiCF_3SO_3$). This particular salt was chosen because of the relative abundance of data available on this system in comparison to other possible electrolytes. The concentration dependence of the conductivity and the transference number were obtained from data available in the literature. The diffusion coefficient of the salt was taken to be constant, since reproducible data were difficult to obtain. Activity coefficient data have not been reported.

The conductivity of PEO-$LiCF_3SO_3$ [19] was fit to a third-order polynomial. The transference number[20] was fit to the equation

$$t_+^0 = 0.0107907 + 1.48837 \times 10^{-4}\, c$$

The diffusion coefficient was taken to be 7.5×10^{-12} m^2/s.[20] The solubility limit of lithium trifluoromethane sulfonate in PEO was assumed to occur at the transition from amorphous behavior to mixed-phase behavior on the phase diagram for this system, leading to $c_{max} = 3920$ mol/m^3.[6]

APPENDIX B

Superposition

Since the equations describing transport in the active cathode material are linear, contributions to the flux from a series of step changes in surface concentration can be superposed. This is an example of Duhamel's superposition integral

$$\frac{\partial c_s}{\delta r}(R_s, t) = \int_0^t \frac{\partial c_s}{\partial t}(R_s, \zeta)\, \frac{\partial \bar{c}_s}{\partial r}(R_s, t-\zeta)\, d\zeta \qquad [B\text{-}1]$$

where $\bar{c}$ represents the solution to Eq. 13 for a unit step change in concentration at the surface. The above integral is calculated numerically using the method suggested by Wagner[21] and by Acrivos and Chambré.[22] Where

$$\frac{\partial c_s}{\partial r}(R_s, t) = \sum_{k=0}^{n-2} \frac{(c_{s,k+1} - c_{s,k})}{\Delta t} A_{n-k} + \frac{(c_{s,n} - c_{s,n-1})}{\Delta t} A_1 \qquad [B\text{-}2]$$

where

$$A_{n-k} = a[(n-k)\Delta t] - a[(n-k-1)\Delta t] \qquad [B\text{-}3]$$

and

$$a(t) = \int_0^t \frac{\partial \bar{c}_s}{\partial r}(R_s, \zeta)\, d\zeta \qquad [B\text{-}4]$$

Two expressions for $a(t)$ were developed with Laplace transforms: at long times

$$a(\tau) = \frac{2}{\pi^2} \sum_{n=1}^{\infty} \frac{1}{n^2} [1 - \exp(-n^2\pi^2\tau)] \qquad [B\text{-}5]$$

and for short times

$$a(\tau) = -\tau + 2\left(\frac{\tau}{\pi}\right)^{1/2} \left[1 + 2\sum_{n=1}^{\infty} \exp\left(\frac{-n^2}{\tau}\right) - n\left(\frac{\pi}{\tau}\right)^{1/2} \operatorname{erfc}\left(\frac{n}{\sqrt{\tau}}\right)\right] \qquad [B\text{-}6]$$

τ is dimensionless time; $\tau = tD_s/R_s^2$. These expressions are each uniformly valid; however, the latter expression converges more quickly with fewer terms at very short times. The values of $a(\tau)$ and A_{n-k} can be calculated separately and used whenever Eq. B-2 must be evaluated. This procedure, applicable to linear diffusion into the cathode matrix, is consequently more efficient than solving for the two-dimensional transport directly.

LIST OF SYMBOLS

a	specific interfacial area, m^2/m^3
c	concentration of electrolyte, mol/m^3
c_0	concentration of polymer solvent, mol/m^3
c_i	concentration of species i, mol/m^3
c_T	maximum concentration in solid, mol/m^3
c_s	concentration in solid, mol/m^3
c_{max}	maximum concentration in polymer, mol/m^3
c^o	initial concentration in polymer, mol/m^3
D, D_s	diffusion coefficient of electrolyte in the polymer and of lithium in the solid matrix, m^2/s
f	activity coefficient
F	Faraday's constant, 96,487 C/eq
$\mathbf{i}$	current density, A/m^2

Downloaded on 2018-05-24 to IP 128.122.230.148 address. Redistribution subject to ECS terms of use (see ecsdl.org/site/terms_use) unless CC License in place (see abstract).

i_o exchange current density, A/m^2
I superficial current density, A/m^2
j_n pore wall flux of lithium ions, mol/m^2 · s
k_2 reaction rate constant at cathode/polymer interface, m^4/mol · s
k_{a1} anodic reaction rate constant, m^3/s
k_{c1} cathodic reaction rate constant, m^3/s
K_{ij} frictional coefficient, J · s/m^5
n number of electrons transferred in electrode reaction
$\mathbf{N}_i$ molar flux in x direction of species i, mol/m^2 · s
r distance normal to surface of cathode material, m
R universal gas constant, 8.3143 J/mol · K
R_s radius of cathode material, m
s_i stoichiometric coefficient of species i in electrode reaction
S dimensionless ratios defined in Eq. 26 and 27
t time, s
t_i^0 transference number of species i
T temperature, K
u utilization of intercalation material
U open-circuit potential, V
$\mathbf{v}_i$ velocity of species i, m/s
V cell potential, V
x distance from the anode, m
$\bar{x}$ dimensionless distance from the anode
z_i charge number of species i
α_a, α_c transfer coefficients
β activity coefficient correction
δ dimensionless current density
δ_s thickness of separator, m
δ_c thickness of composite cathode, m
ϵ porosity of electrode
ζ activity coefficient correction, or dummy variable of integration, s
η surface overpotential, V
Θ_p site concentration in polymer
Θ_s site concentration in solid matrix
κ conductivity of electrolyte, S/m
ν dimensionless exchange current density
ν_+, ν_- number of cations and anions into which a mole of electrolyte dissociates
σ conductivity of solid matrix, S/m
τ dimensionless time
μ_i electrochemical potential of species i, J/mol
Φ electrical potential, V

Subscripts

c cathode
r reference state
s solid phase, or separator
T maximum concentration in intercalation material
1 solid matrix
2 solution phase

Superscripts

0 solvent, or initial condition
θ standard cell potential

REFERENCES

1. A. Hooper and J. M. North, *Solid State Ionics,* **9&10,** 1161 (1983).
2. F. Bonino, M. Ottaviani, B. Scrosati, and G. Pistoia, *This Journal,* **135,** 12 (1988).
3. M. Gauthier, D. Fauteux, G. Vassort, A. Belanger, M. Duval, P. Ricoux, J.-M. Chabagno, D. Muller, P. Rigaud, M. B. Armand, and D. Deroo, *ibid.,* **132,** 1333 (1985).
4. M. Z. A. Munshi and B. B. Owens, *Solid State Ionics,* **26,** 41 (1988).
5. K. M. Abraham, *J. Power Sources,* **7,** 1 (1981/1982).
6. F. M. Gray, *Solid Polymer Electrolytes,* VCH, New York (1991).
7. D. Fauteux, *Solid State Ionics,* **17,** 133 (1985).
8. K. West, T. Jacobsen, and S. Atlung, *This Journal,* **129,** 1480 (1982).
9. M. A. Ratner, in *Polymer Electrolyte Reviews-1,* J. R. MacCallum and C. A. Vincent, Editors, Elsevier Applied Science, London (1987).
10. R. Pollard and J. Newman, *Electrochim. Acta,* **25,** 315 (1980).
11. M. B. Armand, in *Polymer Electrolyte Reviews-1,* J. R. MacCallum and C. A. Vincent, Editors, Elsevier Applied Science, London (1987).
12. J. Newman, *Electrochemical Systems,* Prentice-Hall, Englewood Cliffs, NJ (1991).
13. T. F. Fuller and J. Newman, *This Journal,* **139,** 1332 (1992).
14. C. A. C. Sequeira and A. Hooper, *Solid State Ionics,* **9&10,** 1131 (1983).
15. J. Newman and W. Tiedemann, *AIChE J.,* **21,** 25 (1975).
16. S. Basu and W. L. Worrell, in *Fast Ion Transport in Solids,* P. Vashista, J. N. Mundy, and G. K. Shenoy, Editors, p. 149, North-Holland Publishing Co., Amsterdam (1979).
17. B. C. H. Steele, G. E. Lagos, P. C. Spurdens, C. Forsyth, and A. D. Foord, *Solid State Ionics,* **9&10,** 391 (1983).
18. R. Pollard and J. Newman, *This Journal,* **128,** 503 (1981).
19. D. Fauteux, *ibid.,* **135,** 2231 (1988).
20. A. Bouridah, F. Dalard, D. Deroo, and M. B. Armand, *J. Appl. Electrochem.,* **17,** 625 (1987).
21. C. Wagner, *J. Mathematics and Physics,* **34,** 289 (1954).
22. A. Acrivos and P. L. Chambrè, *Ind. Eng. Chem.,* **49,** 1025 (1957).

Downloaded on 2018-05-24 to IP 128.122.230.148 address. Redistribution subject to ECS terms of use (see ecsdl.org/site/terms_use) unless CC License in place (see abstract).